Current Optics and Photonics
Vol. 4, No. 2, April 2020, pp. 95-102

ISSN: 2508-7266(Print) / ISSN: 2508-7274(Online)
DOI: https://doi.org/10.3807/COPP.2020.4.2.095

The Impact of Deflection on the Sensing Response of Fiber Bragg Gratings Bonded to Graphene and PMMA Substrates

Younis Mohammed Salih[1], Mudhaffer Mustafa Ameen[2], Fahmi F. Muhammadsharif[3]*, Mohammad Fadhli Ahmad[1], Nor Aieni Haji Mokhtar[1], Ismael Mohammed Mohammed Saeed[4], Md Nurul Islam Siddique[1], Ahmad Nazri Dagang[1], Salisa Abdul Rahman[1], Nurul Adilah Abdul Latiff[1], and Abd Khamim Ismail[5]

[1]School of Ocean Engineering Technology and Informatics, Universiti Malaysia Terengganu, 21030 Kuala Nerus, Terengganu, Malaysia
[2]Department of Physics, Faculty of Education, Tishk International University, 44001 Erbil, IRAQ
[3]Department of Physics, Faculty of Science and Health, Koya University, 44023 Koya, Kurdistan Region-F.R., Iraq
[4]Department of Physics, College of Educational Science, University of Garmian, 46021 Kalar, Kurdistan Region-Iraq
[5]Department of Physics Faculty of Science, Universiti Teknologi Malaysia, Skudai, 81310 Johor, Malaysia

(Received October 11, 2019 : revised January 17, 2020 : accepted February 12, 2020)

The impact of graphene and poly(methyl methacrylate) (PMMA) substrates on the response of a fiber Bragg grating (FBG) due to mechanical deflection was investigated. For this purpose, four FBGs with grating lengths of 5, 15, 25, and 35.9 mm were utilized. Higher sensitivity was found for FBGs of larger grating length and for those bonded to graphene substrate. It was concluded that FBGs of smaller grating length (5 and 15 mm) were more sensitive in compression mode, while those of larger grating length (25 and 35.9 mm) were seen to be highly sensitive in tension mode.

Keywords : FBG sensitivity, Mechanical deflection, Graphene, PMMA, Bonded FBG
OCIS codes : (060.3738) Fiber Bragg gratings; (120.4880) Optomechanics; (160.4890) Organic materials; (060.4510) Bragg reflectors; (160.2290) Fiber materials

I. INTRODUCTION

A fiber Bragg grating (FBG) is defined as a small segment of optical fiber that is capable of transmitting all wavelengths except specific ones that are reflected [1, 2]. An FBG is obtained by producing periodic or quasiperiodic changes in the refractive index of the core of a single-mode optical fiber. This periodic variation in refractive index is basically achieved by irradiating the core of the fiber with an interference pattern of ultraviolet light. In this manner, the pattern is imprinted into the fiber [3, 4]. The FBG has found itself in a variety of applications such as measuring dynamic strain, ultrasound detection, pressure measurement, temperature monitoring in building architecture, ultraviolet sensors, and microwave generation [5-17]. It can be also used for maintenance in flight condition monitoring, space vehicles, and in marine and medical science [18, 19]. Its application has been further extended to provide real-time monitoring of cracks or leaks in reactor-vessel-head penetration in a nuclear power plant (NPP) [20, 21]. The use of FBG for strain measurement has drawn a lot of attention from researchers, owing to its unique properties such as effectiveness and simplicity, compared to other types of optical fibers [22]. According to the literature, wide application of FBGs can be due to their ability to retain reflectivity under radiation exposure, and their

*Corresponding author: fahmi982@gmail.com, ORCID 0000-0002-4563-9671
Color versions of one or more of the figures in this paper are available online.

immunity to electromagnetic interference [23, 24].

Researchers have tried various strategies to enhance the sensitivity of FBGs. For instance, Seo *et al.* reported that cantilever sensors are capable of exhibiting a highly sensitive resonance-frequency spectrum [25]. Subsequently, Lee *et al.* used copper/carbon and copper-coated fiber to develop a FBG acoustic sensor for integrated structural health monitoring (ISHM) of a nuclear power plant (NPP) [21, 26]. By carrying out a full three-dimensional numerical analysis and experimental verification of an acoustic sensor in the frequency range from 0.5 to 30 kHz, Moccia *et al.* showed the first evidence of the resonant behavior of an underwater acoustic sensor of an FBG coated by a ring-shaped material [27]. To produce tension and compression in FBGs, Fayed *et al.* used a rapidly variable electromagnetic force [28], while Mavoori *et al.* employed a magnetic actuator [29], and Iocco *et al.* utilized a piezoelectric actuator [30]. Furthermore, a motorized actuator was used to produce axial strain in either tension or compression mode [29]. On the other hand, Goh *et al.* applied a beam-bending method [31], in which a cantilever beam with applied lateral strain was used to produce the tension and compression [32-35]. Linear-displacement measurement is specifically important, whereby a number of configurations for FBG strain sensors have been demonstrated [36-38].

The selection of suitable materials presenting high flexibility and excellent curvature deviation, for the purpose of producing a systematic deflection in the FBG, is of great importance. A graphene sheet has very high mechanical strength, yet can be easily stretched. Ma *et al.* emphasized that with such unique characteristics of graphene [39, 40], it is possible to build miniature pressure and acoustic sensors with high sensitivity and dynamic range. Graphene provides outstanding properties that can be integrated into various flexible and stretchable electronic devices, in a conventional and scalable fashion [41]. The mechanical properties of graphene make it an attractive candidate for applications in strain sensing. Graphene-based materials have shown gauge factors among the highest reported values, enhancing the elongation range of strain sensors from stretches of a few percent to several hundred percent [41]. In this research, the sensing response of FBGs bonded to graphene and poly(methyl methacrylate) (PMMA) sheets is investigated versus the changes in mechanical deflection. Four FBGs of various grating lengths (5, 15, 25 and 35.9 mm) are utilized, and their response is measured under tension and compression modes of an applied tensile stress. The remainder of this paper is organized as follows: the methodology of materials preparation, device setup, and measurement are presented in section II, while the achieved results are discussed in section III, followed by the drawing of the main conclusions in section IV.

II. METHODS

2.1. Preparation of the FBG Bonded to a Graphene Sheet on PMMA Substrate

To prepare the FBG bonded to graphene on a PMMA substrate, a desired area of 74×26 mm^2 from 150-mm long

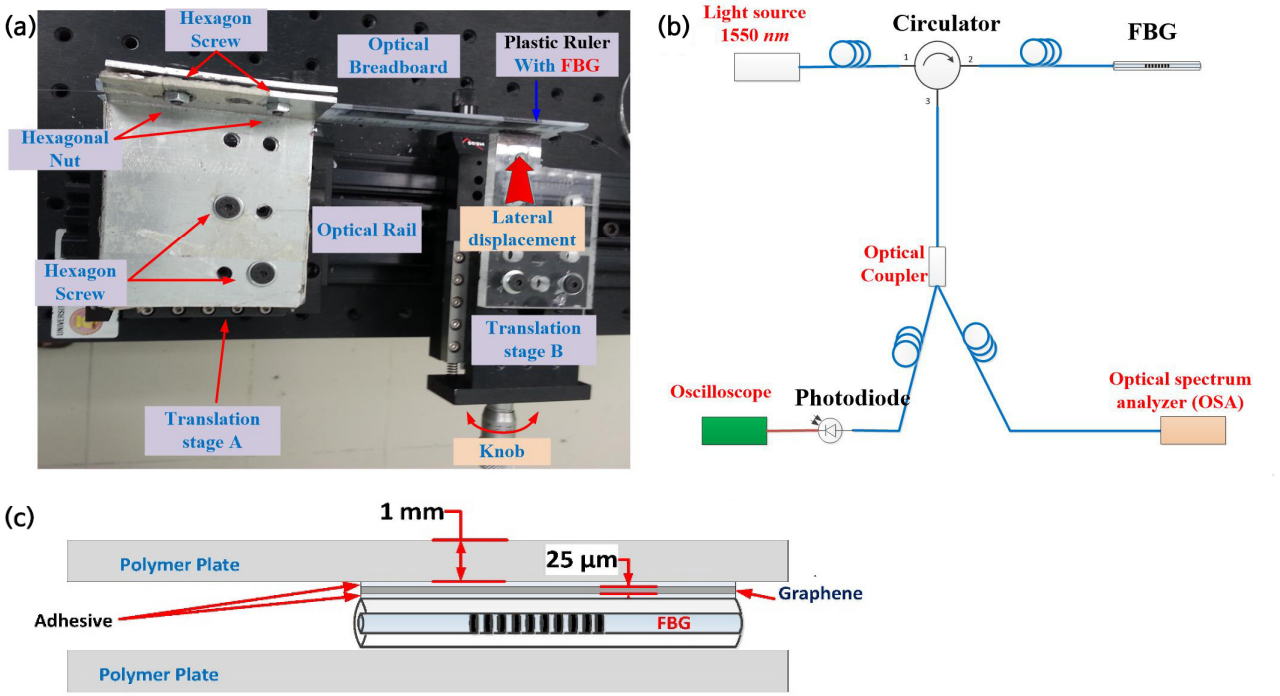

FIG. 1. Experimental setup for (a) measuring the strain and (b) recording the reflected spectrum and average output voltage simultaneously, and (c) a schematic diagram describing the structure of the FBG-bonded sensor.

of PMMA substrate, having a thickness of 1 mm, was used to bond the FBG sensors. This was done using a specified adhesive material of the SELLEEYS type to bond the FBG horizontally onto the surface of the graphene sheet. The specifications of the graphene sheet are as follows: carbon content 97%, thickness 25 μm, density 2 g/cm^3, thermal conductivity (*x*-*y* plane) 1300~1500 W m^{-1} K^{-1} (z plane) 13~15 W m^{-1} K^{-1}, tensile strength 30 MPa, sheet resistance 2.8×10^{-2} Ω/square. The SELLEEYS adhesive was used to affix the graphene sheet upon the PMMA substrate. The FBG-bonded sensors were sandwiched between graphene/PMMA on one side and PMMA on the other side. Figure 1(c) presents a schematic diagram describing structure of the FBG-bonded sensor.

2.2. Experimental Setup for Measuring the Strain

To produce tension and compression deflections in the FBG-bonded sensor, two translation stages were used, as shown in Fig. 1(a). Using aluminum plate, the sensor was screwed down at one end of translation stage A. Rotation of the knob results in a linear displacement of the translation stage B, in micrometers. By this means, the curvature of the PMMA substrate can be increased or decreased, which in turn deflects the FBG in tension or compression mode. An external amplified spontaneous emission (ALS-18-B-FA ASE) light source with a spectral range from 1452 to 1652 nm, operating at its maximum power of 1.83 mW, was used to obtain the response of the FBG. The response was recorded for both the FBG bonded to a graphene sheet and the FBG bonded to graphene/PMMA, in two modes. Considering that the FBG was attached to the front of the PMMA substrate, the compression mode was realized by applying a lateral displacement *d* to the back of the substrate, while the tension mode was achieved by applying a lateral displacement to the front of the substrate. The displacement was made possible by linear translation stage B (see Fig. 1). To analyze the obtained results and assess the performance of the FBG sensors, the sensitivity of the sensors was measured under different physical conditions. In previous studies, optimum FBG performance was seen with the FBG sensor under stress at a location of 3 cm [42]. Therefore, in these experimental investigations the analysis of the FBG bonded to graphene on PMMA was carried out when the FBG sensors were subjected to different lateral displacements, under compression and tension modes, with the stress location fixed at the optimal value of 3 cm.

2.3. Correlation between Optical and Electrical Outputs of FBG Bonded to Graphene

Attempts have been made to estimate the correlation between the system's reflected power and average output voltage. This objective was realized using the same procedures and experimental setups presented in subsection 2.2; the only difference was that a 3-dB coupler was connected to port 3 of the circulator and extended to a high-speed photodiode and an optical spectrum analyzer through ports 1 and 2 respectively, while the photodiode was used in conjunction with an oscilloscope, as illustrated in Fig. 1(b).

The area under the curve of average output voltage versus lateral displacement was determined as follows: two different baselines were created for the reflected spectrum, and then the average of the areas at the two baselines was considered. The first baseline was generated at the bottom of the broad peak, and the second was taken at 90% of the first. Each baseline is defined by a segment connecting λ_1 to λ_2, respectively the initial and final points of the baseline along the abscissa, as shown in Fig. 2.

Consequently the average area under the curve for the reflected spectrum of optical power versus lateral displacement was plotted for all grating lengths (5, 15, 25, and 35.9 mm) of the bonded FBGs, in compression and tension modes. The normalized output voltage and area were calculated by assuming a value of zero for the first measurement, while subtracting the actual first value from each of the subsequent measurements.

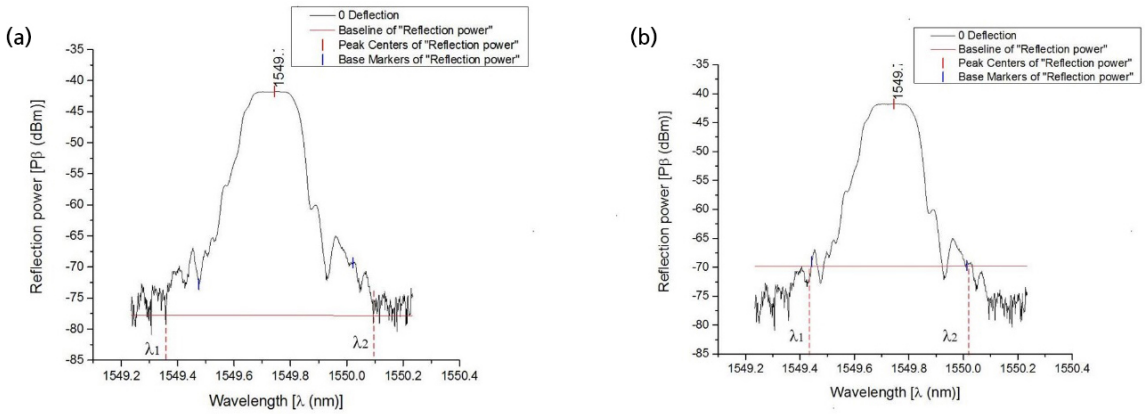

FIG. 2. Illustration of (a) the first assigned baseline and (b) the second assigned baseline, which are used to measure the area under the curve.

III. RESULTS AND DISCUSSION

3.1. Sensitivity of FBGs Bonded to PMMA and Graphene/PMMA under Tension and Compression

The normalized average output voltage of the bonded FBGs versus linear lateral displacement, in both compression and tension modes, was recorded following the methodology described in section 2.3. The obtained results are shown in Fig. 3, where it can be seen that the reflected output voltage increases when lateral displacement is increased at different stress locations for the FBGs of 25-mm grating length, under tension and compression. The relationship between output voltage and lateral displacement was found to be almost linear for the FBGs bonded to PMMA substrate and deflected at stress locations of 1 and 2 cm. However, at the far stress location of 3 cm, the FBGs bonded to graphene/PMMA showed a nonlinear correlation. As such, two distinct regions I and II were observed, in which the sensitivity of the FBGs was found to differ: The sensitivity in the low-deflection region was higher than that in the high-deflection region. This can be safely ascribed to the stiffness of the graphene/PMMA system. In the low-deflection region, the elasticity of the graphene sheet prevailed over that of the PMMA, while in the high-deflection region the elastic response of the PMMA dominates. From the sensitivity measurement, the optimum response was guven by the FBG bonded to graphene/PMMA. It is worth mentioning that the sensitivity at the 3-cm stress location was higher than those at the other locations, for both modes. Notably, the increase in voltage with FBG deflection is highly responsive when the stress location is far from the fixed end of the FBG, elaborating that the deflection impact is effectively distributed across the area of the bonded FBG, which in turn leads to increased reflection power. Hence the farthest possible stress location of 3 cm was chosen.

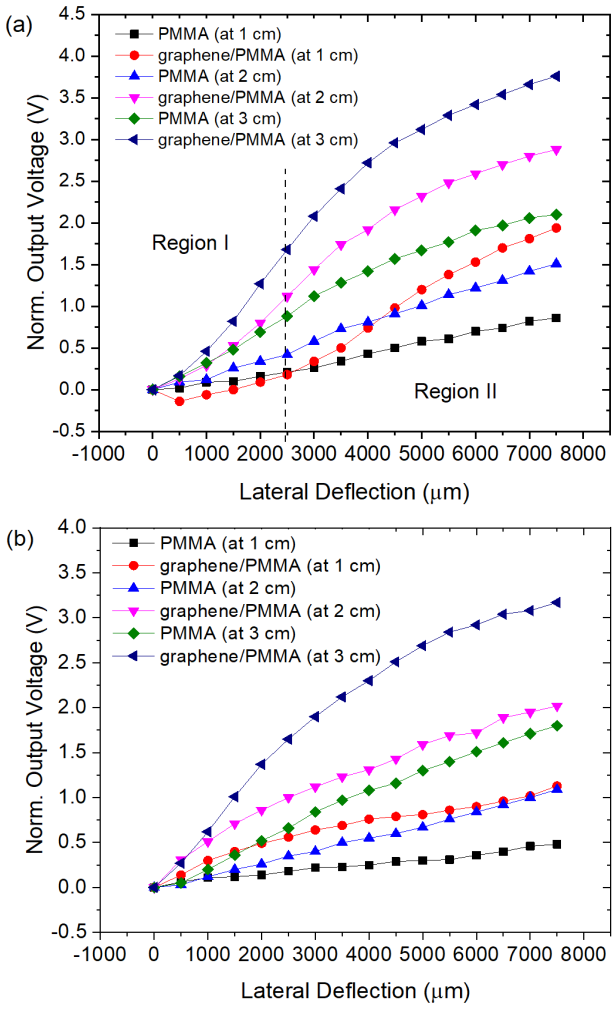

FIG. 3. The normalized output voltage for the FBG (1549.39 nm) with 25-mm grating length, under (a) tension and (b) compression, for different applied-stress locations.

3.2. Sensitivity of FBG Sensors with Different Grating Lengths under Compression and Tension

The normalized average output voltage versus linear lateral displacement of FBGs bonded to graphene/PMMA was measured following the methodology described in section 2.3. The FBG grating lengths were 5, 15, 25, and 35.9 mm [43-46], and the FGBs were deflected at 3 cm.

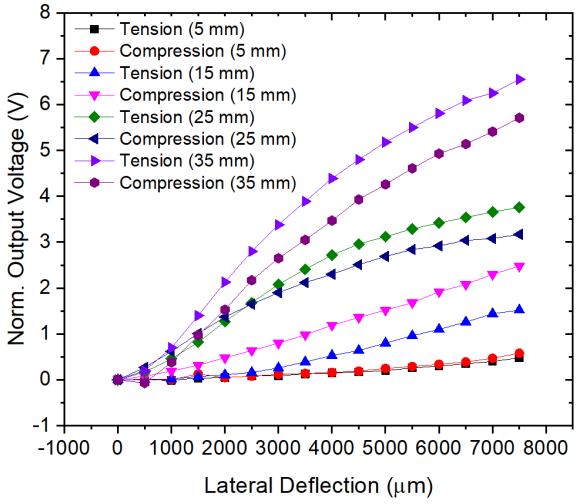

FIG. 4. The normalized output voltage versus linear lateral displacement for the FBGs bonded to graphene/PMMA, under compression and tension, with stress applied at 3 cm.

TABLE 1. The variation of sensitivity for grating lengths of 5, 15, 25, and 35.9 mm, under tension and compression, for the FBGs bonded to graphene/PMMA substrate

Physical condition	Sensitivity × 10^{-4} (V.μm^{-1})			
	5 mm	15 mm	25 mm	35.9 mm
Tension	0.619	2.200	5.390	9.300
Compression	0.719	3.410	4.280	8.270

Figure 4 shows the average output voltage versus linear lateral displacement for all grating lengths of the FBG bonded to graphene/PMMA, under tension and compression. One can notice from the figure that the output voltage rose with increasing grating length, which is attributed to the increase in reflected output power coming from the larger grating lengths, yielding higher output voltage detcted by the oscilloscope.

The sensitivity of the FBGs with various grating lengths, under tension and compression, was calculated from the slope of the output voltage using the Origin Pro 9 software, as tabulated in Table 1. Note that for the smaller grating lengths of 5 and 15 mm, the response in compression mode is better than that in tension mode, while for the larger grating lengths of 25 and 35.9 mm the FBG response in tension mode wasbetter. Notably, this change for the FBG with grating length of 15 mm under compression was very linear, showing a regression coefficient of determination R^2 of 0.99374. It was observed that the sensitivity in tension mode was different than that in compression mode. This can be due to that one face of the FBG is bonded to the graphene sheet, and hence a bilateral deflection of different sensitivities is yield, which can be fruitfully utilized for various applicants. Consequently, in the low-deflection region, the sensitivity of FBGs under compression was larger than for those under tension, while in the high-deflection region the opposite trend was observed.

3.3. Output Power of the Reflected Signal under Deflected Tension and Compression

Figure 5 shows the reflected spectrum of the FBGs with various grating lengths, for tension stress applied at 3 cm. One can notice from the results a clear, broad band shift toward longer wavelengths (redshift) when the FBGs are tensioned. This is in good agreement with theoretical expectations and with previous findings reported by other researchers [25, 33]. Moreover, it was observed that area under the reflected curve increased with increasing tension, indicating an enlarged signal of reflected power with increased mechanical deflection. The variation in reflected

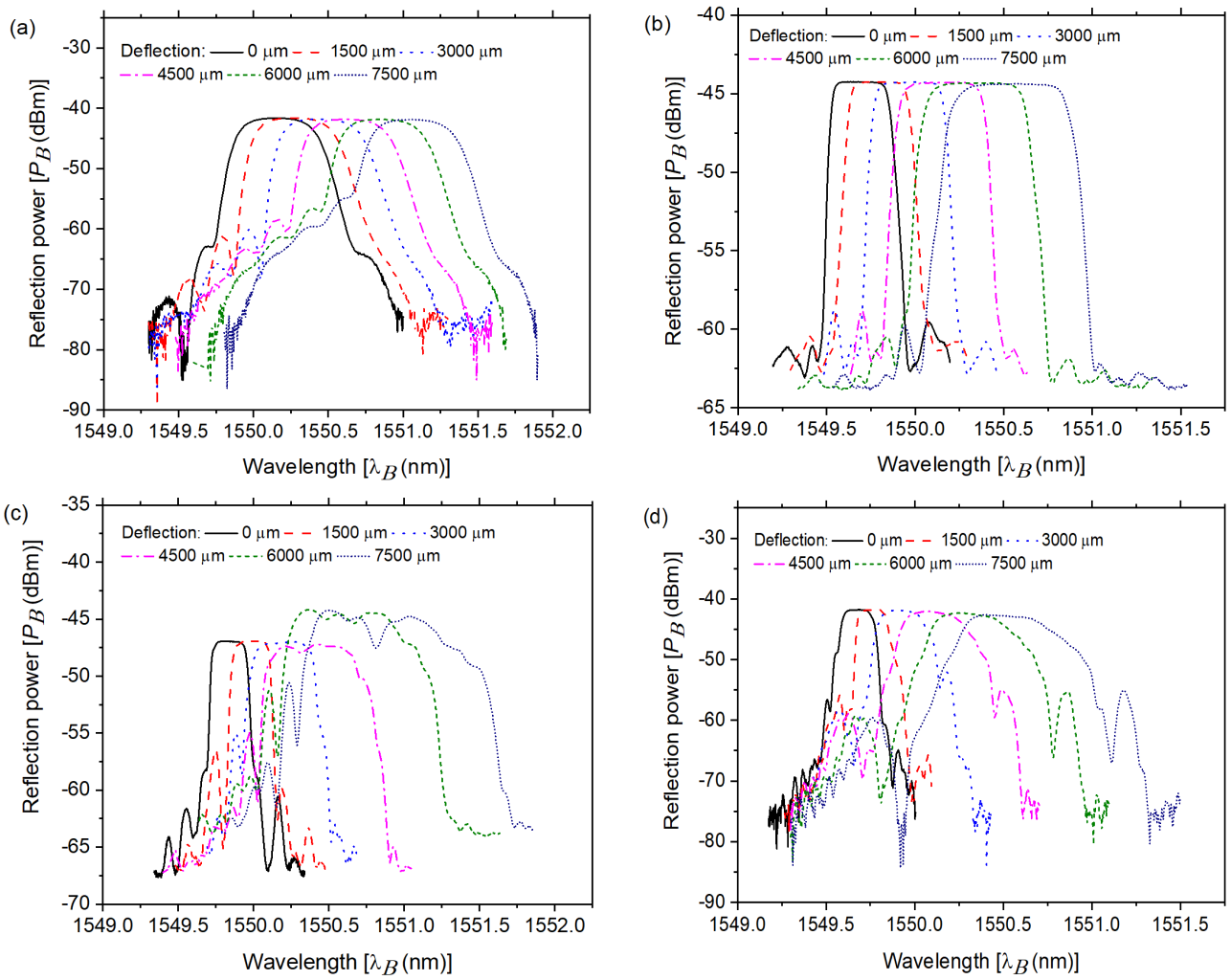

FIG. 5. Reflected power spectra of the FBGs with grating lengths of (a) 5 mm, (b) 15 mm, (c) 25 mm, and (d) 35.9 mm, induced by different lateral displacements due to tension.

TABLE 2. The variation of the area under the reflection curve versus tension deflection, for various grating lengths of FBG sensors bonded to graphene/PMMA substrate

d (μm)	Area under curve (a.u.)^2			
	5 mm	15 mm	25 mm	35.9 mm
0	0.00	0.00	0.00	0.00
1500	0.38	0.71	0.24	0.29
3000	0.50	1.79	3.25	6.53
4500	1.40	3.40	8.07	12.53
6000	3.25	8.39	15.97	18.81
7500	5.19	10.16	19.61	24.19

TABLE 3. The variation of the area under the reflection curve versus compression deflection, for various grating lengths of FBG sensors bonded to graphene/PMMA substrate

d (μm)	Area under curve (a.u.)^2			
	5 mm	15 mm	25 mm	35.9 mm
0	0.00	0.00	0.00	0.00
1500	1.11	1.54	3.23	3.72
3000	1.90	4.05	6.59	8.40
4500	3.71	7.66	9.43	12.08
6000	4.72	11.07	12.69	14.12
7500	6.84	14.81	15.56	15.60

power for the FBGs at high lateral deflection can be attributed to inhomogeneity in the FBG's internal structure, which is dominant at high deflections, thereby deteriorating the reflected spectrum peak. Noteworthy is the pronounced change in the area under the reflected spectrum, which is ascribed to birefringence [48, 49].

The results shown in Tables 2 and 3 present an increase in the average area under the reflection curve for all FBGs, under both tension and compression. The output power reflected from the FBG increased with increasing lateral displacement, due to the increment in the area under the reflection curve. Since the integrated area represents the output reflected power coming from the FBG, the total output reflected power received by the photodiode is therefore increased.

IV. CONCLUSION

The presented sensitivity analysis of FBGs revealed that bonding the FBGs to graphene/PMMA substrate led to improved sensitivity performance, under both tension and compression. Higher sensitivity was found for FBGs of larger grating length, and for those bonded to graphene. It was concluded that FBGs with small grating lengths of 5 and 15 mm performed better in compression mode, whereas FBGs with larger gratings length of 25 and 35.9 mm were more responsive in tension mode. The general trend in sensitivity change was seen to be similar for different FBGs. However, this change for the FBG of grating length 15 mm under compression was the most linear, showing a regression coefficient of determination R^2 of 0.99374.

ACKNOWLEDGMENT

The authors acknowledge financial support from Universiti Malaysia Terengganu, the Malaysian Ministry of Higher Education, and Universiti Teknologi Malaysia under GUP vote number Q.J130000.2509.08H40 for this research work.

REFERENCES

1. K. O. Hill and G. Meltz, "Fiber Bragg grating technology fundamentals and overview," J. Lightwave Technol. **15**, 1263-1276 (1997).
2. W. W. Morey, G. Meltz, and W. H. Glenn, "Fiber optic Bragg grating sensors," Proc. SPIE **1169**, 98-107 (1990).
3. J. Skaar, "Synthesis and characterization of fiber Bragg gratings," Ph. D. Dissertation, Norwegian University of Science and Technology, Norway (2000), pp. 1-2.
4. S. A. Mastro, "Optomechanical behavior of embedded fiber Bragg grating strain sensors," Ph. D. Dissertation, Drexel University, USA (2005).
5. S. Choi, S.-L. Lee, J. Kim, S. J. Jeong, M. S. Kim, D. Kim, and Y. W. Lee, "High sensitivity polarimetric optical fiber pressure sensor based on tapered polarization-maintaining and fiber Bragg grating," J. Nanosci. Nanotechnol. **19**, 1403-1409 (2019).
6. S. Liang, S. C. Tjin, B. Lin, X. Sheng, S. Lou, Y. Zhang, and X. Wang, "Novel fiber Bragg grating sensing method based on the sidelobe modulation for ultrasound detection," J. Lightwave Technol. **37**, 2686-2693 (2019).
7. E. Vorathin, Z. M. Hafizi, A. M. Aizzuddin, and K. S. Lim, "A highly sensitive multiplexed FBG pressure transducer based on natural rubber diaphragm and ultrathin aluminium sheet," Opt. Laser Technol. **106**, 177-181 (2018).
8. E. Vorathin, Z. M. Hafizi, A. M. Aizzuddin, and K. S. Lim, "A natural rubber diaphragm based transducer for simultaneous pressure and temperature measurement by using a single FBG," Opt. Fiber Technol. **45**, 8-13 (2018).
9. E. Vorathin, Z. M. Hafizi, A. M. Aizzuddin, M. K. A. Zaini, and K. S. Lim, "Temperature-independent chirped FBG pressure transducer with high sensitivity," Opt. Lasers Eng. **117**, 49-56 (2019).
10. H. Wu, Q. Lin, Z. Jiang, F. Zhang, L. Li, and L. Zhao, "A temperature and strain sensor based on a cascade of double fiber Bragg grating," Meas. Sci. Technol. **30**, 065104 (2019).
11. F. Yu, Y. Okabe, Q. Wu, and N. Shigeta, "Fiber-optic sensor-based remote acoustic emission measurement of composites," Smart Mater. Struct. **25**, 105033 (2016).
12. L. Htein, Z. Liu, B. Zhou, and H.-Y. Tam, "Bragg grating in novel two-core holey fiber for simultaneous measurement

of pressure and temperature," in *Proc. IEEE Opto-Electronics and Communications Conference (OECC) and Photonics Global Conference (PGC)* (Singapore, Jul. 2017), pp. 1-2.
13. H.-N. Li, D.-S. Li, and G.-B. Song, "Recent applications of fiber optic sensors to health monitoring in civil engineering," Eng. Struct. **26**, 1647-1657 (2004).
14. Y.-B. Lin, T.-K. Lin, Y.-H. Kuo, L. Wang, and K.-C. Chang, "Application of FBG sensors to strain and temperature monitoring of full scale prestressed concrete bridges," in *Proc. IEEE 15th Optical Fiber Sensors Conference Technical Digest. OFS 2002 (Cat. No.02EX533)* (OR, USA, May 2002), pp. 211-214.
15. M. Matin, N. Hussain, and R. Shoureshi, "Fiber Bragg sensor for smart bed sheet," Proc. SPIE **5907**, 590706 (2005).
16. G.-S. Seo and T.-J. Ahn, "Protection Method for Diameter-downsized Fiber Bragg Gratings for Highly Sensitive Ultraviolet Light Sensors," Curr. Opt. Photon. **2**, 221-225 (2018).
17. Z. Xiaobo, C. Yiwang, Z. Pin, Y. Qin, N. Jiazheng, and D. Xiaohua, "Tunable low phase-noise microwave generation utilizing an optoelectronic oscillator and a fiber Bragg grating," Curr. Opt. Photon. **2**, 96-100 (2018).
18. N. Miesen, Y. Mizutani, R. M. Groves, J. Sinke, and R. Benedictus, "Lamb wave detection in prepreg composite materials with fibre Bragg grating sensors," Proc. SPIE **7981**, 79812J (2011).
19. T. H. T. Chan, L. Yu, H.-Y. Tam, Y.-Q. Ni, S. Liu, W. H. Chung, and L. K. Cheng, "Fiber Bragg grating sensors for structural health monitoring of Tsing Ma bridge: Background and experimental observation," Eng. Struct. **28**, 648-659 (2006).
20. G. Rajan, S. Jinachandran, J. Xi, H. Li, J. S. Vinod, T. Moses, S. Karekal, and B. G. Prusty, "Fibre optic acoustic emission measurement technique for crack activity monitoring in civil engineering applications," in *Proc. IEEE Sensors Applications Symposium (SAS),* (Catania, Italy, Apr. 2016), pp. 1-6.
21. J. R. Lee, S. Y. Chong, C. Y. Yun, and H. Sohn, "Design of fiber Bragg grating acoustic sensor for structural health monitoring of nuclear power plant," Adv. Mater. Res. **123-125**, 859-862 (2010).
22. R. Ramalingam, R. Nast, and H. Neumann, "Strain characterization of high temperature superconductor tapes using embedded fibre Bragg grating sensor in mid-rip and parallel configuration," J. Supercond. Nov. Magn. **30**, 1963-1970 (2017).
23. Y. Liu, L. Li, L. Zhao, J. Wang, and T. Liu, "Research on a new fiber-optic axial pressure sensor of transformer winding based on fiber Bragg grating," Photonic Sens. **7**, 365-371 (2017).
24. V. R. Pachava, S. Kamineni, S. S. Madhuvarasu, K. Putha, and V. R. Mamidi, "FBG based high sensitive pressure sensor and its low-cost interrogation system with enhanced resolution," Photonic Sens. **5**, 321-329 (2015).
25. D.-C. Seo, D.-J. Yoon, I.-B. Kwon, and S.-S. Lee, "Sensitivity enhancement of fiber optic FBG sensor for acoustic emission," Proc. SPIE **7294**, 729415 (2009).
26. S. Y. Chong, J.-R. Lee, C.-Y. Yun, and H. Sohn, "Design of copper/carbon-coated fiber Bragg grating acoustic sensor net for integrated health monitoring of nuclear power plant," Nucl. Eng. Des. **241**, 1889-1898 (2011).
27. M. Moccia, M. Pisco, A. Cutolo, V. Galdi, P. Bevilacqua, and A. Cusano, "Opto-acoustic behavior of coated fiber Bragg gratings," Opt. Express **19**, 18842-18860 (2011).
28. H. A. Fayed, M. Mahmoud, A. K. A. Seoud, and M. H. Aly, "A wide range tunable fiber Bragg grating using fast changeable electromagnetic force," Proc. SPIE **7750**, 77501R (2010).
29. S. Jin, H. Mavoori, R. Espindola, L. Adams, and T. Strasser, "Magnetically tunable fiber Bragg gratings," in *Optical Fiber Communication Conference and the International Conference on Integrated Optics and Optical Fiber Communication* (Optical Fiber Communication Conference, 1999), pp. ThJ2.
30. A. Iocco, H. G. Limberger, R. P. Salathe, L. A. Everall, K. E. Chisholm, J. A. Williams, and I. Bennion, "Bragg grating fast tunable filter for wavelength division multiplexing," J. lightwave technol. **17**, 1217 (1999).
31. C. S. Goh, M. Mokhtar, S. Butler, S. Y. Set, K. Kikuchi, and M. Ibsen, "Wavelength tuning of fiber Bragg gratings over 90 nm using a simple tuning package," IEEE Photonics Technol. Lett. **15**, 557-559 (2003).
32. Z. Qin, Q. Zeng, X. Yang, D. Feng, L. Ding, G. Kai, Z. Liu, S. Yuan, X. Dong, and N. Liu, "Bidirectional grating wavelength shifter with a broad-range tunability by using a beam of uniform strength," IEEE Photonics Technol. Lett. **13**, 326-328 (2001).
33. M.-K. Kang, D.-J. Park, and S.-S. Lee, "Strain measurements on a cantilever beam with fiber Bragg grating sensors using a pair of collimators," Int. J. Precis. Eng. Man. **13**, 455-458 (2012).
34. Y. Yu, H. Tam, S. Geng, M. S. Demokan, Z. Liu, and W. Chung, "Chirp-free tuning of fiber Bragg grating using a cantilever beam," Jpn. J. Appl. Phys. **38**, L1032 (1999).
35. K. Feng, J. Cui, X. Jiang, J. Li, and J. Tan, "Analysis and simulation method of the cantilever FBG sensors," Proc. SPIE **9903**, 99031E (2016).
36. Y. Mizutani and R. M. Groves, "Multi-functional measurement using a single FBG sensor," Exp. Mech. **51**, 1489-1498 (2011).
37. J. Waldbjørn, J. Høgh, J. Wittrup-Schmidt, M. W. Nielsen, K. Branner, H. Stang, and C. Berggreen, "Strain and displacement controls by fibre Bragg grating and digital image correlation," Strain **50**, 262-273 (2014).
38. M. H. Yau, "Vertical displacement measurement using fibre Bragg grating (FBG) sensors for structural health monitoring of bridges," Ph. D. Thesis, Queensland University of Technology, Australia (2014).
39. J. Ma, W. Jin, H. L. Ho, and J. Y. Dai, "High-sensitivity fiber-tip pressure sensor with graphene diaphragm," Opt. Lett. **37**, 2493-2495 (2012).
40. O. F. Ameen, M. H. Younus, M. S. Aziz, A. I. Azmi, R. K. R. Ibrahim, and S. K. Ghoshal, "Graphene diaphragm integrated FBG sensors for simultaneous measurement of water level and temperature," Sens. Actuators, A **252**, 225-232 (2016).
41. H. Jang, Y. J. Park, X. Chen, T. Das, M. S. Kim, and J. H. Ahn, "Graphene-based flexible and stretchable electronics," Adv. Mater. **28**, 4184-4202 (2016).
42. Y. M. Salih, Y. Munajat, A. K. Ismail, and H. Bakhtiar, "Response of FBG-bonded plastic plate at different locations

of applied stress," J Teknol. **78**, 77-83 (2016).
43. M. Hernaez, C. R. Zamarreño, S Melendi-Espina, L. R. Bird, A. G. Mayes, and F. J. Arregui, "Optical fibre sensors using graphene-based materials: A review," Sensors **17**, 155 (2017).
44. Sridevi. S, K. S. Vasu, S. Asokan, and A. K. Sood, "Enhanced strain and temperature sensing by reduced graphene oxide coated etched fiber Bragg gratings," Opt. Lett. **41**, 2604-2607 (2016).
45. I. L. Justino, A. R. Gomes, A. C. Freitas, A. C. Duarte, T. A. P. Rocha-Santos, "Graphene based sensors and biosensors," TrAC, Trends Anal. Chem. **91**, 53-66 (2017).
46. Y. Zhao, X.-g. Li, X. Zhou, Y. Zhang, "Review on the graphene based optical fiber chemical and biological sensors," Sens. Actuators B Chem. **231** 324-340 (2016).
47. R. Gafsi and M. A. El-Sherif, "Analysis of induced-birefringence effects on fiber Bragg gratings," Opt. Fiber Technol. **6**, 299-323 (2000).
48. J. Molimard, S. Vacher, and A. Vautrin, "Monitoring LCM process by FBG sensor under birefringence," Strain **47**, 364-373 (2011).
49. W. Zhang, W. Chen, Y. Shu, X. Lei, and X. Liu, "Effects of bonding layer on the available strain measuring range of fiber Bragg gratings," Appl. Opt. **53**, 885-891 (2014).